



1 **Response of protonated, adduct, and fragmented ions in Vocus proton-**
2 **transfer-reaction time-of-flight mass spectrometer (PTR-ToF-MS)**

3

4 Fangbing Li¹, Dan Dan Huang², Linhui Tian¹, Bin Yuan³, Wen Tan⁴, Liang Zhu⁴,
5 Penglin Ye⁵, Douglas Worsnop⁵, Ka In Hoi¹, Kai Meng Mok¹, Yong Jie Li¹

6 ¹Department of Civil and Environmental Engineering, Department of Ocean Science
7 and Technology, and Centre for Regional Oceans, Faculty of Science and Technology,
8 University of Macau, Macau, China

9 ²State Environmental Protection Key Laboratory of Cause and Prevention of Urban Air
10 Pollution Complex, Shanghai Academy of Environmental Sciences, Shanghai, China

11 ³Institute for Environment and Climate Research, Jinan University, Guangzhou 510632,
12 China

13 ⁴Tofwerk AG, Nanjing, China

14 ⁵Aerodyne Research, Inc., Billerica, Massachusetts 01821, United States

15 *Correspondence to:* Yong Jie Li (yongjieli@um.edu.mo)

16



17 **Abstract**

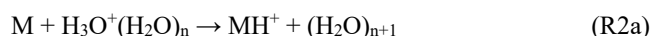
18 Volatile organic compounds (VOCs) affect secondary pollutant formation via active
19 chemistry. Proton-transfer-reaction mass spectrometry (PTR-MS) is one of the most
20 important techniques to study the highly variable spatial and temporal characteristics
21 of VOCs. The response of protonated, adduct, and fragmented ions in PTR-MS in
22 changing instrument settings and varying relative humidity (RH) requires rigorous
23 characterization. Herein, dedicatedly designed laboratory experiments were conducted
24 to investigate the response of these ions for 21 VOCs, including 12 oxygenated VOCs
25 and two nitriles, using the recently developed Vocus PTR-MS. Our results show that
26 the focusing ion-molecule reactor (FIMR) axial voltage increases sensitivity by three
27 to four orders of magnitude but does not significantly change the fractions of protonated
28 ions. Reducing the FIMR pressure, however, substantially increases fragmentation.
29 Applying a high radio frequency (RF) amplitude radially on FIMR can enhance
30 sensitivity by one to two orders of magnitude without affecting the protonated ion
31 fractions. The change in big segmented quadrupole (BSQ) amplitude mainly affects
32 sensitivity and protonated ion fraction by modifying ion transmission. The relationship
33 between sensitivity and proton-transfer reaction rate constant is complicated by the
34 influences from both ion transmission and protonated ion fraction. The protonated ions
35 of most VOCs studied (19 out of 21) show less than 15% variations in sensitivity as RH
36 increases from ~5% to ~85%, except for some long-chain aldehydes which show a
37 positive RH variation of up to 30%. Our results suggest that the Vocus PTR-MS can
38 reliably quantify the majority of VOCs under ambient conditions with varying RH.
39 However, caution is advised for small oxygenates such as formaldehyde and methanol
40 due to their low sensitivity, as well as for long-chain aldehydes for their slight RH
41 dependence and fragmentation.

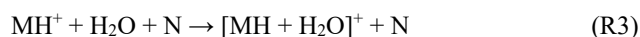
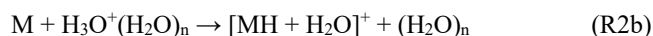


42 **1 Introduction**

43 Atmospheric volatile organic compounds (VOCs) affect atmospheric chemistry by
44 forming secondary pollutants such as tropospheric O₃ (Shao et al., 2016) and secondary
45 organic aerosols (SOA) (Shrivastava et al., 2017). In addition to their low mixing ratios
46 (parts per billion by volume, ppbv, or even lower), the spatial and temporal variabilities
47 of atmospheric VOCs pose another analytical challenge to the study of their
48 atmospheric occurrence, sources, and fates. Mass spectrometric (MS) techniques based
49 on ion-molecule reactions (IMR) (Španěl and Smith, 1996) or specifically proton-
50 transfer reactions (PTR) (Hansel et al., 1995; Lindinger et al., 1998) in a selected ion
51 flow tube (SIFT) have been developed to provide fast-responding measurements of
52 VOCs. These techniques, especially the PTR-MS, have been widely used in VOC
53 measurements in outdoor and indoor environments (Salazar Gómez et al.,
54 2021; Sekimoto and Koss, 2021; Pagonis et al., 2019; Pleil et al., 2019; Clafflin et al.,
55 2021; Schripp et al., 2014; Jensen et al., 2021).

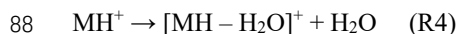
56 Quantification of VOCs (denoted as M) by PTR-MS relies heavily on their proton-
57 transfer reactions with the hydronium ion H₃O⁺ (R1). In early SIFT-MS studies where
58 reagent ions include a multitude of H₃O⁺(H₂O)_n (n = 0, 1, 2, 3...) ion series (Španěl and
59 Smith, 2000), proton-transfer reactions with more hydrated (n ≥ 1) hydronium ions
60 (R2a) are also important for species with proton affinity (PA) larger than water clusters.
61 In addition, ligand switching reactions (R2b) and association reactions (R3, with N
62 being N₂ or O₂) are also common, leading to [MH + H₂O]⁺ instead of MH⁺. Under these
63 circumstances, the quantification of VOCs might be heavily influenced by water vapor
64 concentration, or relative humidity (RH), of the sample. For instance, acetone
65 concentrations in exhaled air were overestimated by 13% even using both protonated
66 (MH⁺) and water adduct ([MH + H₂O]⁺) ions for quantification, when water vapor
67 varied in the range of (1 – 10) × 10¹² molecules cm⁻³ (Španěl and Smith, 2000). A later
68 study (Smith et al., 2001) showed that quantification of other oxygenated VOCs
69 (OVOCs) such as ethyl acetate, diethyl ether, methanol, ethanol, and propanol by SIFT-
70 MS also suffered from RH dependence to various degrees.



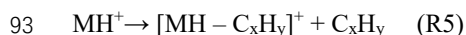


71 For PTR-MS that normally uses the MH^+ for quantification, RH dependence was
72 also widely reported. For instance, Warneke et al. (2001) reported that the sensitivity of
73 benzene in PTR-MS decreased significantly with the increase of RH, while Steinbacher
74 et al. (2004) suggested a slight decrease with the increase of RH. Quantification of
75 biogenic volatile organic compounds (BVOCs) was also reported to be slightly affected
76 by RH (Kari et al., 2018). The RH dependence stems from the change of reagent ion
77 distribution, i.e., among H_3O^+ and $H_3O^+(H_2O)_n$ ($n \geq 1$), which can lead to
78 overestimation or underestimation of VOCs if such dependence is strong because
79 ambient RH is deemed highly variable. Therefore, RH-dependent calibrations for VOC
80 measurements using PTR-MS were normally recommended (de Gouw and Warneke,
81 2007;Inomata et al., 2008;Sinha et al., 2009;Vlasenko et al., 2010;Cui et al.,
82 2016;Michoud et al., 2018).

83 Another complication in VOC measurements using SIFT-MS or PTR-MS is that,
84 due to the nucleophilicity of the oxygen atom, protonated OVOCs would dehydrate,
85 forming fragmented ions (R4). This reaction often occurs in heavy alcohols, aldehydes,
86 and carboxylic acids (Španěl et al., 1997;Španěl and Smith, 1998;Hartungen et al.,
87 2004;Baasandorj et al., 2015).



89 In addition, cleavage on the C-C bond of the protonated ion (R5) is also possible,
90 especially for alkyl-substituted VOCs under high-energy conditions (e.g., a high E/N
91 ratio, which is the reduced electric field parameter with E being the electric field and N
92 the number density of the gas in the drift tube).



94 For instance, at an E/N ratio of 120 Townsend (Td), substituted monocyclic aromatic
95 compounds such as ethylbenzene and propylbenzene start to fragment into a benzenium
96 ion ($C_6H_7^+$) (de Gouw et al., 2003;Gueneron et al., 2015).

97 A newly designed focusing ion-molecule reactor (FIMR) was used for PTR-MS,
98 termed Vocus, and has been shown to have little RH dependence for the protonated ion
99 because of the high concentration of water vapor introduced into the drift tube



100 (Krechmer et al., 2018). The concentration of hydronium ion (H_3O^+) in the drift tube is
101 high enough to maintain at a constant level and dominate over other side reactions,
102 thereby minimizing the RH dependence for VOC measurement. Yet, the formation of
103 adduct ions and fragmented ions in Vocus PTR-MS as a function of RH has not been
104 fully scrutinized, hindering a complete understanding of the ion chemistry in the Vocus
105 PTR-MS and potential cross interference when measuring ambient air with complex
106 VOC mixtures. Herein, we conducted experiments on the effects of instrumental
107 settings and RH variations on the quantification of 21 VOCs, including 12 OVOCs and
108 2 nitriles, using a Vocus PTR-MS. Response of protonated ions (MH^+), adduct ions
109 ($[\text{MH} + \text{H}_2\text{O}]^+$), and fragmented ions ($[\text{MH} - \text{H}_2\text{O}]^+$ or $[\text{MH} - \text{C}_x\text{H}_y]^+$) of these VOCs
110 was investigated as a function of instrumental setting and RH. Results are interpreted
111 based on the PA values and/or proton-transfer reaction rate constants (k_{ptr}). Some
112 caveats on using the Vocus PTR-MS to measure VOCs, especially OVOCs, are also
113 provided.

114 **2 Methodology**

115 **2.1 Instrument settings**

116 Experiments were performed with a Vocus proton-transfer-reaction time-of-flight
117 mass spectrometer (PTR-ToF-MS, Vocus 2R, TOFWERK AG, Thun, Switzerland),
118 hereinafter referred to as Vocus. The Vocus consists of (i) a discharge ion source, (ii) a
119 focusing ion-molecule reactor (FIMR), (iii) a big segmented quadrupole (BSQ), (iv) a
120 series of direct current (DC) optics that further focus and accelerate the primary beam
121 (PB), and (v) a time-of-flight (ToF) mass analyzer (Krechmer et al., 2018). The ion
122 source is a plasma discharge composed of two conical surfaces. Water vapor is supplied
123 by purging 20 to 30 mL of milli-Q water and is ionized by plasma discharge. The
124 reagent ions pass through a ring offset from the central axis so that the photons
125 generated by the discharge cannot enter. The drift tube was improved by replacing the
126 stacked ring electrodes of the traditional PTR-MS with a FIMR, which is a glass tube
127 with a resistive coating on the inner surface and a quadrupole with a radio frequency
128 (RF) electric field applied. The FIMR increases ion transmission by a factor of 7 to 9
129 and sensitivity by more than one order of magnitude (Krechmer et al., 2018). Moreover,
130 the mean kinetic energy of H_3O^+ is increased by three times, and the formation of more
131 hydrated hydronium ions is reduced, suppressing RH dependence for most VOCs



132 measured (Krechmer et al., 2018). Meanwhile, the mean kinetic energy of VOCs
133 measured is not significantly increased, thereby minimizing fragmentation (Krechmer
134 et al., 2018). The ToF mass analyzer offers a mass resolving power of 12,000 at a mass-
135 to-charge ratio (m/Q) of 107 Thomson (Th).

136 In our experiments, sample air was drawn into the instrument using 0.5 m long
137 perfluoroalkoxy (PFA) Teflon tubing of ~0.5 m length and 1/4" outer diameter, with a
138 flow rate of 0.5 L·min⁻¹. Most of the sample air was directed to the exhaust, while the
139 actual flow into the FIMR was around 0.15 L·min⁻¹. In typical experiments, the drift
140 tube was operated at a pressure of 2.0 mbar and a temperature of 373.15 K. The axial
141 and radial voltages were normally set to be 625 and 500 V, respectively, unless stated
142 otherwise.

143 We also performed experiments by varying the instrument settings such as FIMR
144 axial voltage (V) and FIMR pressure (p), both of which affect the E/N ratio, as well as
145 RF and BSQ amplitudes to investigate how protonated, adduct, and fragmented ions
146 respond to those changes. These experiments were performed under dry (RH ~5%)
147 conditions, and the concentrations were approximately 12 ppbv for most VOCs (except
148 for β -caryophyllene at about 1.2 ppbv). The instrument settings were varied by: 1)
149 changing the FIMR axial voltage from 260 to 700 volts, 2) changing the pressure in
150 FIMR from 1.5 to 3.5 mbar; 3) changing the RF amplitude from 13 to 500 volts (with
151 p of 2.0 or 3.5 mbar); 4) changing the BSQ voltage from 50 to 300 volts (with p of 2.0
152 or 3.5 mbar). The other instrument settings were fixed as the default values while
153 changing the tested ones. Specifically, RF amplitude was at 500 volts and BSQ
154 amplitude was at 300 volts when changing E (i.e., V) and N (i.e., p), and an E/N ratio
155 of 142 Td was used when changing RF and BSQ amplitudes (Table S1).

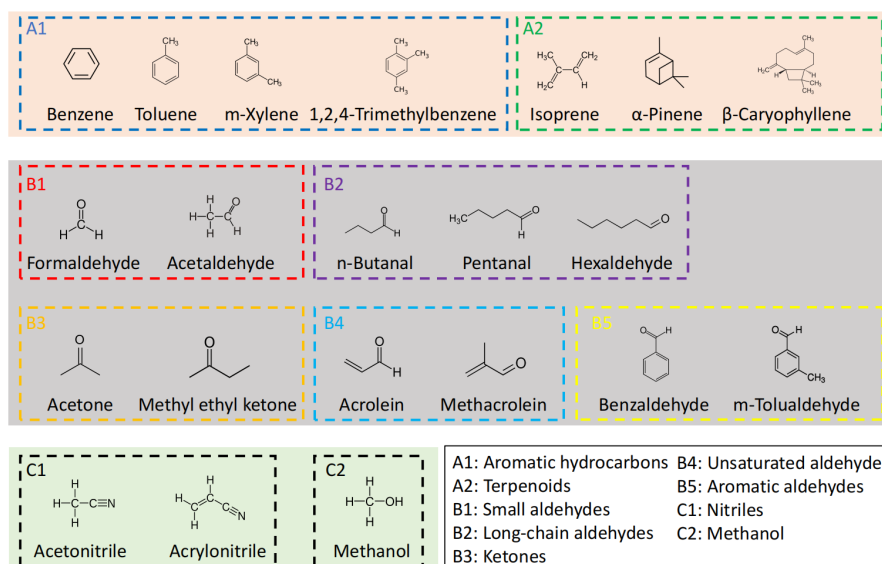
156 2.2 Experimental setup

157 The VOCs (Table S2 and Figure 1) in mixtures from two cylinders were separately
158 delivered to the dilution and/or RH control setup (Figure S1). Dilution air was generated
159 from a zero-air generator (EnviroNics series 7000, EnviroNics Analytics Group Ltd.,
160 Canada). Gas cylinder I (Apel-Riemer Environmental Inc., US, valid for 12 month)
161 contains mainly hydrocarbons, while gas cylinder II (Linde Gases, US, valid for 12
162 month) contains mainly OVOCs and nitriles. Most VOCs in the cylinders are at
163 approximately 1000 ppbv, except for β -caryophyllene that is at approximately 100 ppbv.



164 Table S2 shows their CAS numbers, m/Q values of the protonated ions (MH^+), as well
165 as PA and k_{ptr} values. According to their functional groups, the 21 VOCs are grouped
166 into 9 categories, and Figure 1 shows their structures. Note that although n-butanal and
167 methyl ethyl ketone are isomers, they are in different cylinders and measured separately,
168 thus will not interfere with each other.

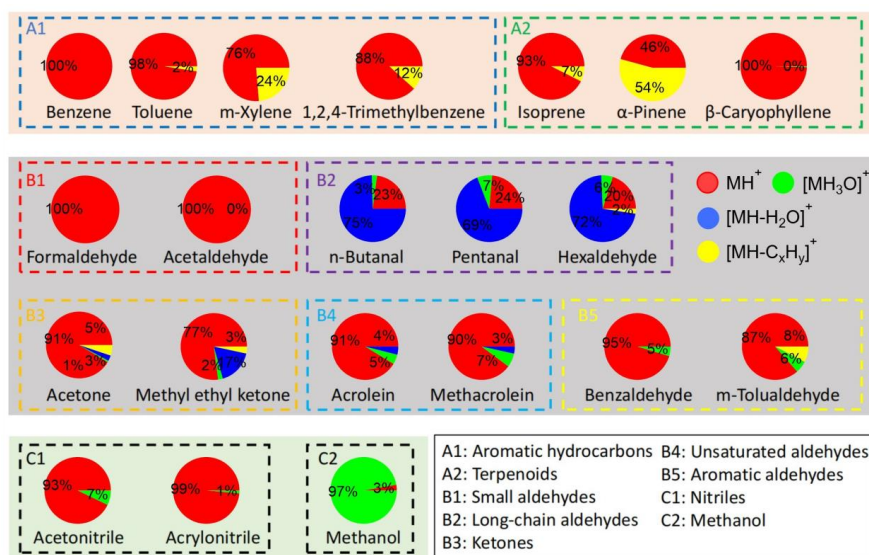
169 Dry experiments were performed by diluting the VOCs from the cylinders with
170 dry zero air with 7 concentrations from 0 to approximately 22 ppbv (or approximately
171 2 ppbv for β -caryophyllene). For each concentration step, measurements lasted for
172 about half an hour for gas cylinder I with hydrocarbons but about two hours for gas
173 cylinder II with OVOCs and nitriles. Other measures such as minimizing the length of
174 the Teflon tube at the inlet (less than 30 cm) were also undertaken to allow fast
175 establishment of equilibrium-state concentrations for OVOCs. In RH-dependent
176 experiments (Figure S1), dilution was made by RH-conditioned air produced from a
177 humidity generator (OHG-4, Owlstone, US). The accuracy of the RH sensor (RH-USB
178 Probe, Omega) is within 4% of RH. Nine RH ramping steps from ~5% to ~85% with
179 approximately 10% intervals were used, and the VOCs were set with 4 concentrations
180 from 0 to approximately 12 ppbv (or approximately 1.2 ppbv for β -caryophyllene).
181 After the initial equilibration of 0.5 hours under dry conditions (RH ~5%), each RH
182 ramping lasted for 15 min. Triplicate experiments were performed for the highest
183 concentration.



184
185 Figure 1. Names, structures, and grouping of the 21 VOCs in this study. These VOCs
186 were prepared in two gas standard cylinders (I and II) with mixing ratios of ~1000 ppbv
187 (~100 ppbv for β -caryophyllene), balanced by N_2 . Acetaldehyde and acetone are
188 present in both gas standard cylinders, with concentrations differing by <5%. n-Butanal
189 and methyl ethyl ketone are isomers but are in different gas standard cylinders.

190 2.3 Data analysis

191 The Vocus data were analyzed with the manufacturer-supplied software package
192 Tofware (v3.2.3) based on Igor Pro (Wavemetrics). Peak fitting was performed using
193 Tofware routines and the measured m/Q values of the protonated ions (MH^+) are shown
194 in Table S2 together with their exact m/Q values. In addition to MH^+ , we also looked
195 for adduct ions ($[MH + H_2O]^+$), and fragmented ions ($[MH - H_2O]^+$ or $[MH - C_xH_y]^+$),
196 since those ions are also anticipated for VOCs, especially OVOCs, in PTR-MS
197 measurements (Pagonis et al., 2019). Although the VOCs were in mixtures and showed
198 ensemble mass spectra, we constructed the mass spectrum for each VOC by plotting
199 their identified adduct or fragmented ions alongside the protonated ions, as shown in
200 Figures S2-S4 in the SI. Their percentage contributions are presented in Figure 2 and
201 numerically in Table S4.



202
 203 Figure 2. The average signal percentages of protonated, adduct, and fragmented ions
 204 at a concentration of ~12 ppbv (~1.2 ppbv for β-caryophyllene).

205 For both dry and RH-dependent experiments, from the 1-minute averages from 1-
 206 Hz datasets, the last five points were averaged to obtain stable signals. Figure S5 shows
 207 the time series of selected hydrocarbons (groups A1 and A2, aromatic hydrocarbons
 208 and terpenoids, Figure S5a) and OVOCs (groups B2 and B5, long-chain and aromatic
 209 aldehydes, Figure S5b) during dry experiments with concentration stepping. Figure S6
 210 shows the time series of protonated ions (MH⁺), adduct ions ([MH + H₂O]⁺), and
 211 fragmented ions ([MH - H₂O]⁺ and/or [MH - C_xH_y]⁺) for n-butanal, pentanal and
 212 hexaldehyde, whose adduct and fragmented ions contributed substantially to the total
 213 signals (Figure 2 and Table S4).

214 Similar to RH-dependent experiments, the duration of each instrument setting
 215 experiment was 15 min. The signal intensities and the ratio of MH⁺, [MH + H₂O]⁺ and
 216 [MH - H₂O]⁺ and/or [MH - C_xH_y]⁺ to all for two typical hydrocarbons (α-pinene and
 217 1,2,4-trimethylbenzene) and two OVOCs (acetone and hexaldehyde) as the axial
 218 voltage and pressure (which both affects the E/N ratio) in the FIMR, RF amplitude, and
 219 BSQ amplitude varied are shown in Figures S7 to S10. The reduced electric field
 220 parameter (E/N ratio) was estimated by comparing the signal fraction of fragment of α-
 221 pinene in Materić et al. (2017), in which detailed examination on fragment signal
 222 fraction at different E/N ratio was performed (Figure S11).



223 2.4 Sensitivity estimation

224 The formation of the protonated ion MH^+ via reaction R1 is desirable for
225 quantification of VOCs, which is described by the kinetics of the proton-transfer
226 reaction (de Gouw and Warneke, 2007; Yuan et al., 2017):

$$227 \quad [MH^+] = [H_3O^+]_0 (1 - e^{-k[M]\Delta t}) \quad (\text{Eq. 1})$$

228 where $[MH^+]$ is the number concentration of the protonated ion, $[H_3O^+]_0$ that of the
229 initial hydronium ion, k is the rate constant of R1 (k_{ptr}), $[M]$ is the number concentration
230 of the target VOCs in the sample air, and Δt is the reaction time in the drift tube. Two
231 conditions allow simplification of Eq. 1 to Eq. 2 below for easy quantification of VOCs:
232 1) The term $k[M]\Delta t$ is much smaller than 1, such that R1 can be considered essentially
233 first-order; and 2) H_3O^+ is not significantly depleted and remain more or less constant
234 after the drift tube. Compared with traditional ion sources, the Vocus ion source
235 produces sufficient H_3O^+ (Krechmer et al., 2018). Ambient levels of ppbv (or less) for
236 $[M]$ ($\sim 10^{10}$ molecule cm^{-3}) generally fulfill such requirements, given that k_{ptr} is on the
237 order of 10^{-9} cm^3 molecule $^{-1}$ s $^{-1}$ and Δt of 10^{-4} s (Ellis and Mayhew, 2014). Therefore,

$$238 \quad [MH^+] = [H_3O^+]k[M]\Delta t \quad (\text{Eq. 2})$$

239 where $[H_3O^+]$ is the mixing ratio of hydronium ions after the drift tube (i.e., being
240 detected in the mass spectrometer). Then,

$$241 \quad [M] = \frac{I_{MH^+}}{I_{H_3O^+}} \frac{1}{k\Delta t} \quad (\text{Eq. 3})$$

242 where I_{MH^+} and $I_{H_3O^+}$ are signal intensities of the protonated ion and the hydronium ion,
243 respectively.

244 In general, the sensitivity (S) of PTR-MS for quantification of VOCs is defined as
245 the ratio between the signal intensity I_{MH^+} normalized by 10^6 cps (counts per second) of
246 $I_{H_3O^+}$ and 1 ppbv (10^{-9} mol mol $^{-1}$) of VOCs, i.e.:

$$247 \quad S = \frac{\frac{I_{MH^+}}{I_{H_3O^+}} \times 10^6}{\frac{[M]}{N} \times 10^9} \quad (\text{Eq. 4})$$



248 where N is the number density of air in the drift tube. The sensitivity S is thus expressed
249 as a normalized signal per ppbv, having a unit of ncps ppbv⁻¹. Combining Eq. 3 and Eq.
250 4 yields,

$$251 \quad S = 10^{-3} \times N \Delta t \times k \text{ (Eq. 5)}$$

252 where $10^{-3} \times N \Delta t$ is specific to the instrumental settings. Eq. 5 dictates that S should
253 have a linear relationship with the proton-transfer reaction rate constant (k_{ptr}) if the
254 instrument settings are fixed and can be utilized to predict S if k_{ptr} values are known
255 (Ellis and Mayhew, 2014).

256 In reality, however, quantification of VOCs using MH^+ from PTR-MS
257 measurements is complicated by 1) formation of adduct (e.g., with H_2O) and
258 fragmented (e.g., dehydration) ions, and 2) discriminated transmission for MH^+ ions
259 with different m/Q values (de Gouw and Warneke, 2007; Yuan et al., 2017). The fraction
260 of MH^+ in all related ions (f_{MH^+}) and the relative transmission efficiency ($T_{\text{MH}^+}/T_{\text{H}_3\text{O}^+}$)
261 are used to account for these two effects, respectively:

$$262 \quad S = 10^{-3} \times N \Delta t \times \frac{T_{\text{MH}^+}}{T_{\text{H}_3\text{O}^+}} \times f_{\text{MH}^+} \times k \text{ (Eq. 6)}$$

263 In our study, the sensitivity is expressed as the slope of signal intensity (in counts
264 per second, cps) vs. concentration (in ppbv), having a unit of cps ppbv⁻¹ (Figure S12).
265 Signal normalization to H_3O^+ (ncps) was not adopted because the signal of H_3O^+ (m/Q
266 = 19 Th) was substantially suppressed with low transmission (see below) for those ions
267 with small m/Q values (but too high intensities) to minimize ion currents.

268 **3 Results and Discussion**

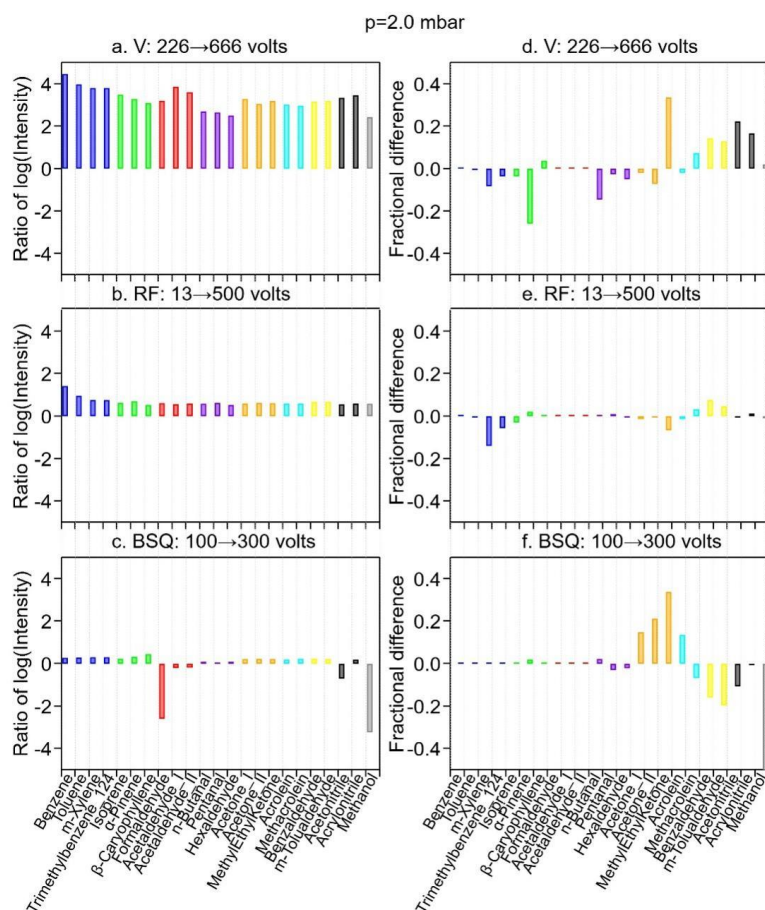
269 **3.1 Effects of instrumental settings on the ion signals**

270 An increase of the E/N ratio from 48 to 142 Td manifested by the increases of the
271 FIMR axial voltage (V, with front from 226 to 666 volts and back keeps at 34 volts) led
272 to drastic increases of MH^+ signal intensity by three to four orders of magnitude for all
273 VOCs studied (Figure 3a). Such increases were also observed for adduct and
274 fragmented ions (Figures S7 - S10), albeit to different extents. It has been shown that
275 increasing the axial voltage in the FIMR can substantially increase protonated ion
276 signals, which is due mainly to three reasons (Krechmer et al., 2018; de Gouw and



277 Warneke, 2007). First, a high FIMR axial voltage can accelerate the ions and thus
 278 reduce their residence time, thereby preventing diffusional loss. Second, the high
 279 voltage in FIMR significantly increases the concentration of all reagent ions (Figure
 280 S13). Lastly, at high voltage, reactions between some OVOCs (such as acetone) and
 281 H_3O^+ leads to more protonated ions (MH^+) instead of adduct ions ($[\text{MH} + \text{H}_2\text{O}]^+$)
 282 through ligand switching reaction (R2b). The last effect was believed to be less
 283 significant for species that do not readily react with $\text{H}_3\text{O}^+(\text{H}_2\text{O})_n$ (such as aromatics and
 284 terpenoids).

■ Aromatic hydrocarbons ■ Terpenoids ■ Small aldehydes ■ Long-chain aldehydes
■ Ketones ■ Unsaturated aldehydes ■ Aromatic aldehydes ■ Nitriles ■ Methanol



285
 286 Figure 3. The ratio of the logarithm of intensity (panels a, b, and c) and the difference
 287 of fractional signal of the protonated ion (MH^+) among all ions (panels d, e, and f),



288 when changing axial voltage (V) or FIMR pressure (p) (panels a and d), RF amplitude
289 (panels b and e), and BSQ amplitude (panels c and f). The ratios were taken after taking
290 the logarithm of the signal intensities of MH^+ at the right-hand side of the instrument
291 setting (after the arrow) to that at the left-hand side of the instrument setting stated in
292 the panel label; likewise, the fractional differences are the fractions of the MH^+ signal
293 among the protonated, fragmented, and adduct signals under these two instrumental
294 settings.

295 To investigate whether the desired MH^+ is indeed more favorably formed by
296 suppressing R2b under high axial voltages, we plot the differences in the signal
297 fractions of MH^+ between axial voltages of 666 volts and 226 volts (Figure 3d). The
298 results show that about one-third of the 21 VOCs do not have significant differences in
299 the signal fractions: most VOCs in this one-third have the MH^+ as the sole or
300 dominating ion observed (*cf.*, Figure 2). Meanwhile, there are about one-third showing
301 negative differences (i.e., decreasing MH^+ fractions) of up to 0.2, including the two
302 hydrocarbons and two OVOCs shown in panel d of Figures S7 – S10. The remaining
303 one-third show positive differences (i.e., increasing MH^+ fractions) of up to 0.3, mainly
304 for unsaturated or aromatic aldehydes, as well as nitriles (Figure 3d). A closer
305 inspection of the fractional changes as axial voltage increases for acetone (Figure S9d)
306 and hexaldehyde (Figure S10d) reveals that the fractions of both MH^+ and $[MH + H_2O]^+$
307 decrease, while those of fragmented ions ($[MH - H_2O]^+$ and/or $[MH - C_xH_y]^+$) increase.
308 The relative decreases of the signal fractions of MH^+ (8% for acetone and 51% for
309 hexaldehyde) are, however, much lower than those of $[MH + H_2O]^+$ (57% for acetone
310 and 80% for hexaldehyde). These observations suggest that while fractions of both MH^+
311 and $[MH + H_2O]^+$ decrease, the decreases of the adduct ion ($[MH + H_2O]^+$) are more
312 significant, supporting the third reason that relatively more H_3O^+ (instead of
313 $H_3O^+(H_2O)_n$) at higher axial voltages to react with these OVOCs. However, as the
314 voltage increases, all ion signals are increasing (Figure S7a-S10a). This observation
315 illustrates that the ion acceleration and diffusion prevention should be the primary
316 reason for signal enhancement at high axial voltages. Nevertheless, the signal fractions
317 of the MH^+ do not change substantially (within 30%) as the FIMR axial voltage
318 increases, making quantification reliable even for species with high signal contributions
319 from adduct and fragmented ions (e.g., long-chain aldehydes, group B2, *cf.*, Figure 2).



320 The increase of E/N ratio by decreasing FIMR pressure from 3.5 to 1.5 mbar
321 increases signal intensities (Figure S14a) of MH^+ by less than one order of magnitude,
322 or even decreases those for some OVOCs such as long-chain aldehydes. The changes
323 in signal fractions of MH^+ (Figure S14d), on the other hand, are more than those when
324 changing axial voltages, especially for ketones, unsaturated aldehydes, aromatic
325 aldehydes, and nitriles. The increase of pressure in the PTR reactor also favors the
326 formation of reagent clusters $\text{H}_3\text{O}^+(\text{H}_2\text{O})_n$, which leads to the formation of adduct ions
327 (Wang et al., 2020). For OVOCs acetone and hexaldehyde, the fractions of MH^+ do
328 increase when FIMR pressure was decreased from 3.5 to 2.5 mbar (E/N ratio from 162
329 to 95), which is accompanied by significant decreases of the adduct ion $[\text{MH} + \text{H}_2\text{O}]^+$
330 (Figure S9j and Figure S10j). This observation suggests less formation of adduct ions
331 at lower FIMR pressures. Further decrease of FIMR pressure to 1.5 mbar, however,
332 results in slight decreases of MH^+ fractions, in lieu of increases of fragmented ions $[\text{MH}$
333 $-\text{H}_2\text{O}]^+$ and $[\text{MH} - \text{C}_x\text{H}_y]^+$ (Figure S9j and Figure S10j); for hydrocarbons α -pinene
334 and 1,2,4-trimethylbenzene (Figure S7j and Figure S8j) that only have MH^+ and $[\text{MH}$
335 $-\text{C}_x\text{H}_y]^+$, continuous decreases of MH^+ fractions and increases of $[\text{MH} - \text{C}_x\text{H}_y]^+$ are
336 observed for the whole range of FIMR pressure tested (3.5 to 1.5 mbar). A recent study
337 using Vocus PTR-MS to measure organic peroxides also observed that less fragmented
338 ions were formed under higher FIMR pressure (Li et al., 2022), presumably due to the
339 efficient transfer of excess kinetic energy by frequent collisions at higher pressures. A
340 medium FIMR pressure of 2.0 mbar was chosen to have relatively low fractions of both
341 adduct ions ($[\text{MH} + \text{H}_2\text{O}]^+$) and fragmented ions ($[\text{MH} - \text{H}_2\text{O}]^+$ and $[\text{MH} - \text{C}_x\text{H}_y]^+$).

342 The radial RF electric field in the FIMR is unique for the Vocus PTR-MS, which
343 can (1) collimate the ions towards the central axis (especially heavier ions) and (2)
344 increase the kinetic energy of the ions (especially for lighter ions) (Krechmer et al.,
345 2018). These effects led to 1 to 1.5 orders of magnitude higher signals for MH^+ at 2.0
346 mbar FIMR pressure (Figure 3b) and 1.5 to 2 orders of magnitude at 3.5 mbar (Figure
347 S14b) when the RF amplitude was changed from 13 to 500 volts. The additional
348 enhancement of signal intensity at a higher FIMR pressure (i.e., 3.5 mbar as compared
349 to 2.0 mbar) can be attributed to a longer residence time of the reagent ions (Krechmer
350 et al., 2018). The more pronounced increase of kinetic energy for lighter ions (e.g.,
351 H_3O^+) than heavier ions [i.e., clusters $\text{H}_3\text{O}^+(\text{H}_2\text{O})_n$] might imply the favorable
352 formation of the protonated ion MH^+ rather than adduct ions. The fractions of MH^+ for



353 different RF amplitudes do not change significantly (within ± 0.2) either at 2.0 mbar
354 (Figure 3e) or 3.5 mbar (Figure S14e). This observation thus suggests that adding the
355 RF can increase signal intensities by 1 – 2 orders of magnitude but does not affect the
356 fractional signal for MH^+ , making it beneficial for accurate quantification.

357 The BSQ amplitude above 100 volts does not change the signal intensities
358 significantly (Figure 3c and Figure S14c, as well as Figures S7– S10). The BSQ ion
359 guide provides a high-pass band filter to reduce the number of ions (thus signal intensity)
360 of low m/Q values (especially for reagent ions, H_3O^+ , with high ion currents),
361 preventing the fast degradation of the microchannel plate (MCP) detector (Krechmer et
362 al., 2018). This bandpass filter leads to lower ion transmission efficiency (< 1) for ions
363 with smaller m/Q values, which is discussed below. Therefore, the signal reduction
364 when the BSQ amplitude increased from 100 to 300 volts is more obvious for small
365 analytes such as formaldehyde, acetonitrile, and methanol (Figure 3c and Figure S14c).
366 For other analytes whose fragmented ions have m/Q values of less than 60 Th, the signal
367 fractions of MH^+ would also be affected (Figure 3f and Figure S14f). For example, the
368 intensities of fragmented ions $[\text{MH} - \text{H}_2\text{O}]^+$ ($\text{CH}_3\text{CCH}_2^+$, $m/Q = 41$ Th) and $[\text{MH} -$
369 $\text{C}_x\text{H}_y]^+$ (CH_3CO^+ , $m/Q = 43$ Th) for acetone had substantial decreases when BSQ
370 amplitude was higher than 200 volts (Figure S9c and Figure S10). The protonated ion
371 MH^+ ($\text{CH}_3\text{COCH}_3\text{H}^+$, $m/Q = 59$ Th) and adduct ion ($\text{CH}_3\text{COCH}_3\text{H}_3\text{O}^+$, $m/Q = 77$ Th),
372 however, remained less unaffected. This effect leads to noticeable changes in signal
373 fractions of MH^+ (maximum 0.4) for small analytes such as ketones, unsaturated
374 aldehydes, nitriles, as well as methanol (Figure 3f and Figure S14f) as the BSQ
375 amplitude changes from 100 to 300 volts.

376 3.2 Sensitivity and transmission of protonated ions

377 We calculated the sensitivity and transmission of protonated ions (MH^+) of the 21
378 VOCs studied when the instrument was under the optimized conditions. Table 1 shows
379 the sensitivities (cps ppbv⁻¹), as slopes of MH^+ signals vs. mixing ratios (average value
380 from 0 to 22 ppbv at dry condition, except for β -caryophyllene to 2 ppbv) and the limit
381 of detection (LOD, 3σ). Panels a and b in Figure 4 show the sensitivity vs. k_{ptr} for all
382 21 VOCs, while panels c and d show the transmission efficiencies calculated from the
383 division of the sensitivity vs. k_{ptr} ratio for each VOC by the slope fitted in Figure 4a and
384 4b.



385 Most VOCs had sensitivities above 1000 cps ppbv⁻¹, except 1) formaldehyde (A2-
 386 1) and methanol (C2-1), whose MH⁺ ions have *m/Q* values much lower than 60 Th; and
 387 2) β-caryophyllene (A2-3) that came with a very low concentration range. In addition
 388 to its low *m/Q* values that limit the transmission, the backward reaction is also an
 389 important reason for the low sensitivity. For instance, formaldehyde has a low PA value
 390 (712.5 kJ mol⁻¹) that is not much higher than that of water (691.0 kJ mol⁻¹) and has been
 391 shown to have a high tendency of backward reaction of R1 (Inomata et al.,
 392 2008;Vlasenko et al., 2010;Warneke et al., 2011). The two compounds in group B5
 393 (aromatic aldehydes), benzaldehyde and m-tolualdehyde, had the highest sensitivities
 394 of >12000 cps ppbv⁻¹. This might be due to their high PA values (>830 kJ mol⁻¹), which
 395 are among the highest except those of terpenoids (Table S2).

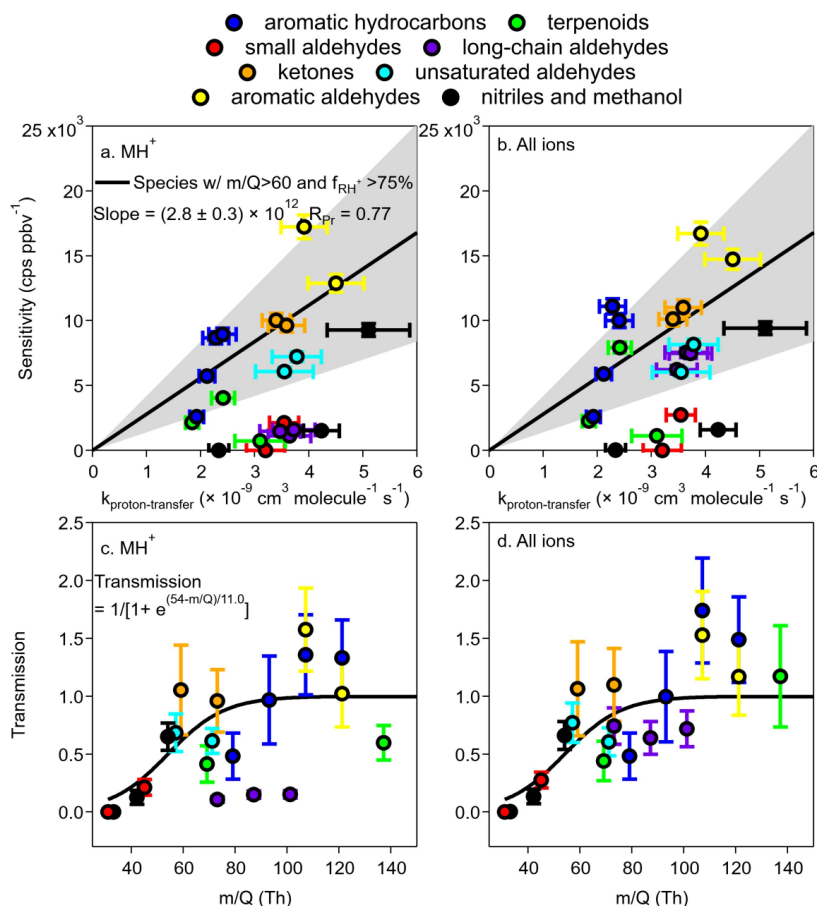
396

397 Table 1. Sensitivity (slope), intercept, and limit of detection (LOD) based on 3 standard
 398 deviations (σ). Results were obtained from measurements of 0 – 22 ppbv for all VOCs
 399 except for β-caryophyllene (up to ~2 ppbv).

Group ^a	Name	Label	Sensitivity (cps ppbv ⁻¹)	3σ LOD (pptv), 5 s
A1	Benzene	A1-1	2596	35
	Toluene	A1-2	5724	2
	m-Xylene	A1-3	8669	3
	1,2,4-Trimethylbenzene	A1-4	8951	1
A2	Isoprene	A2-1	2140	16
	α-Pinene	A2-2	4046	2
	β-Caryophyllene	A2-3	723	1
B1	Formaldehyde	B1-1	— ^c	— ^c
	Acetaldehyde	B1-2	2096 ^b	283
B2	n-Butanal	B2-1	1114	343
	Pentanal	B2-2	1465	63
	Hexaldehyde	B2-3	1595	35
B3	Acetone	B3-1	9932 ^b	127
	Methyl ethyl ketone	B3-3	9636	51
B4	Acrolein	B4-1	7224	16
	Methacrolein	B4-2	6090	13
B5	Benzaldehyde	B5-1	16089	1
	m-Tolualdehyde	B5-2	12893	1
C1	Acetonitrile	C1-1	1511	6
	Acrylonitrile	C1-2	9275	1



400 Notes:
 401 a, A1: aromatic hydrocarbons, A2: terpenoids, B1: small aldehydes; B2: long-chain aldehydes, B3:
 402 ketones, B4: unsaturated aldehydes, B5: aromatic aldehydes, C1: nitriles, C2: methanol;
 403 b, average value from gas standard cylinders I and II;
 404 c, low sensitivity and high LOD due to low transmission.
 405



406 Figure 4. Sensitivity as a function of k_{ptir} for (a) MH^+ and (b) all ions. Linear fitting was
 407 performed only for MH^+ sensitivity. Species included in the fitting were those with m/Q
 408 value > 60 Th (Table S2) and signal percentage of MH^+ (f_{MH^+}) > 75% (Table 1). The
 409 grey-shaded area is bounded by $0.5 \times \text{Slope}$ and $2 \times \text{Slope}$. The fitted curves in panel b
 410 are the same as in panel a and are for reference only. Panels c and d are transmission
 411 curves for MH^+ and all ions. The sigmoidal curve for MH^+ (same for c and d) was fitted
 412 from species except for β -caryophyllene, α -pinene, n-butanal, pentanal, and
 413 hexaldehyde whose fragmentation was significant. Note that only the m/Q values of
 414



415 MH^+ was used in the x axis of panel d, which does not consider the differences in m/Q
416 values of adduct and fragmented ions.

417 It was shown that the sensitivities for different VOCs in PTR-MS can be calculated
418 from the kinetics of the proton-transfer reactions (Warneke et al., 2003; Sekimoto et al.,
419 2017; Cappellin et al., 2012). For Vocus, Krechmer et al. (2018) also pointed out that
420 the relationship between sensitivity and k_{ptr} can be established and used to calculate the
421 sensitivity for other compounds. We herein compare the relationship between
422 sensitivity and k_{ptr} (Figure 4a). In our data, the uncertainties for sensitivity were
423 conservatively taken as the maximum percentage uncertainty (5.3%) of fitted slopes.
424 Values of k_{ptr} were calculated as averages of both modeled and experimental results
425 found from literature (Table S3), with uncertainties propagated from an estimated
426 percentage error of 15% for both modeled (Zhao and Zhang, 2004) and experimental
427 values. The anticipated linear relationship of sensitivity vs. k_{ptr} is not easily visible,
428 most likely due to the formation of fragments/adducts for some VOCs and low
429 transmission efficiencies for others. However, a relatively improved linear relationship
430 was found if we limit the VOCs to 1) m/Q values for $MH^+ > 60$ Th, and 2) a fraction of
431 MH^+ ion in all ions (including adduct/fragmented ions) larger than 75% (*cf.* Figure 2).
432 With these limitations, the fitted linear line gives a slope of $(2.8 \pm 0.3) \times 10^{12}$ cps ppbv⁻¹
433 molec s cm⁻³, approximately 38% lower than that $[(4.5 \pm 0.4) \times 10^{12}$ cps ppbv⁻¹ molec
434 s cm⁻³] of Krechmer et al. (2018). Pearson's R (R_{Pr}) is 0.77. A grey area is also shown
435 by two lines of $2 \times$ slope and $0.5 \times$ slope, which includes approximately half (ten) of
436 the VOCs studied. Those that fall out of the grey area to the lower region are mainly
437 compounds in groups B2 (long-chain aldehydes, purple), C1 and C2 (nitriles or
438 methanol, black), B1 (small aldehydes, red), and A2 (terpenoids, green). Using the total
439 signals of all ions (protonated, adduct, and fragmented), Figure 4b shows the
440 improvements for compounds in group B2 only, while others (especially those in C1,
441 C2, and B1) do not move up to the grey area.

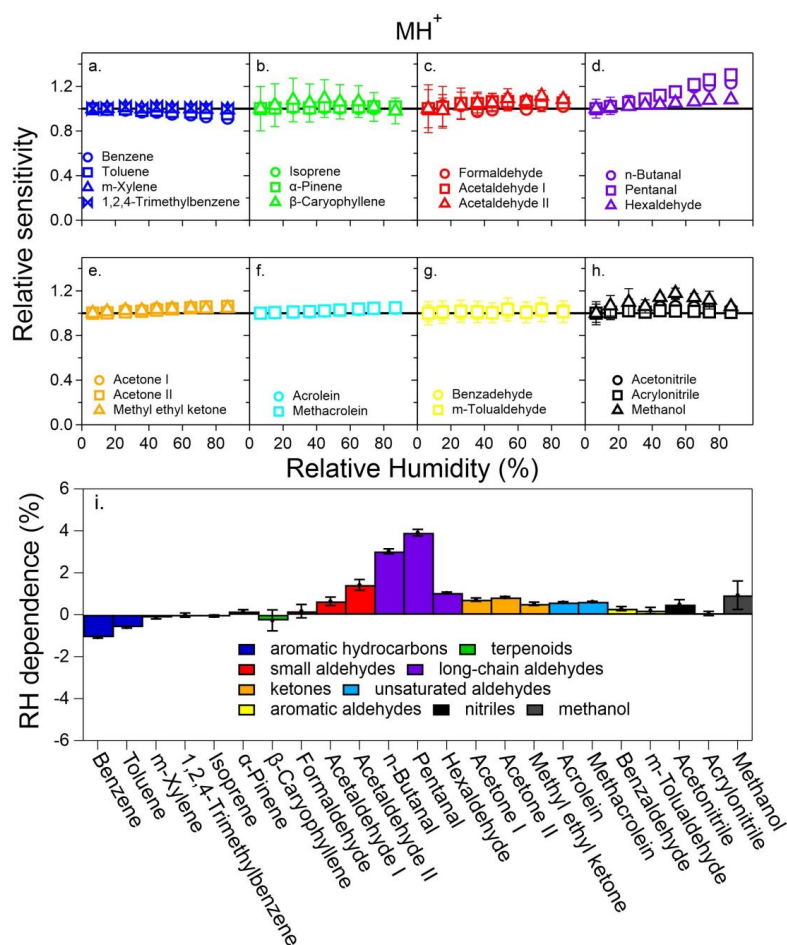
442 We also calculated the transmission efficiencies (Figure 4c and 4d) from the
443 division of the sensitivity vs. k_{ptr} ratio for each VOC by the slope fitted in Figure 4a. It
444 is shown that compounds in groups B1, C1, and C2 are mainly on the rising range of
445 the sigmoidal curve, while the three long-chain aldehydes in group B2 (purple) are well
446 below the curve if only MH^+ ions were used; these three long-chain aldehydes move up
447 to transmission > 0.5 when all ions are considered (Figure 4d). Of particular interest is



448 the compound α -pinene, whose transmission was < 0.5 when only the MH^+ ion was
449 used, but it increases to about 1.5 when the fragmented ion was considered. Note that
450 in Figure 4d, the m/Q value of MH^+ was used in the x axis for the summed ion signals,
451 which might lead to certain bias as the fragmented and adduct ions have different m/Q
452 values. Nevertheless, the above analysis suggests that both the formation of
453 adduct/fragmented ions and transmission affect the relationship between sensitivity and
454 k_{ptr} , which needs precaution when using predicted sensitivity directly from k_{ptr} . In
455 addition, one needs to be cautious about the prediction of transmission efficiency with
456 m/Q greater than 150.

457 3.3 RH dependence of ion signals

458 One of the most important reasons for RH dependence is that the distribution of
459 reagent ions might vary with ambient RH, especially when the abundance of H_3O^+ in
460 the PTR reactor is not high. While the Vocus has been shown to have abundant enough
461 H_3O^+ (Krechmer et al., 2018), whether it can substantially minimize RH dependence
462 for most VOCs deserves scrutinization. Figure 5a-h shows the relative sensitivity,
463 defined as the relative change of sensitivity of MH^+ ion vs. VOC concentration under
464 different RH conditions. Among the nine groups of VOCs studied, seven groups show
465 almost flat relative sensitivities within the RH range of $\sim 5\%$ to $\sim 85\%$ (298 K), with the
466 exceptions of long-chain aldehydes (group B2) that show increasing sensitivities as RH
467 increases (Figure 5d) and methanol (group C2) showing large variations (Figure 5h).
468 Some other compounds, such as β -caryophyllene (A2-3, Figure 5b) and formaldehyde
469 (B1-1, Figure 5c) also show either relatively large uncertainties or fluctuations, which
470 can be ascribed to their low intensities (*cf.*, Table 1).

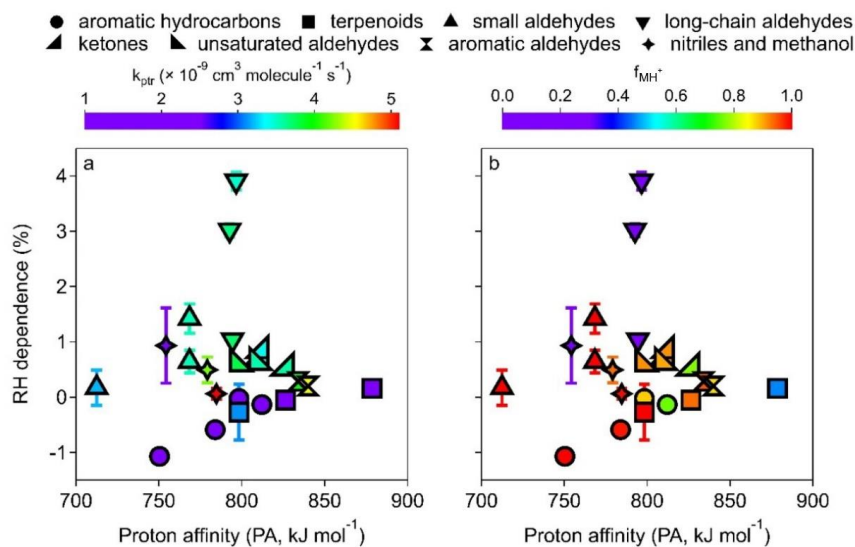


471
472 Figure 5. The dependence of the MH^+ signals on RH for the VOCs studied. Panels a-h:
473 the relative sensitivity was calculated as the slope (Sensitivity) under all conditions to
474 that at the dry ($RH < 5\%$) condition. Panel i: the percent change of relative sensitivity
475 per 10% RH increase. See Figures S15-S17 for other ion signals.

476 Figure 5i shows the RH dependence of the MH^+ ions, defined as the percentage
477 change of sensitivity per 10% RH increase, for all 21 VOCs studied. Aromatic
478 hydrocarbons (group A1) show negative RH dependence as in previous studies using
479 PTR-MS with a drift tube (Warneke et al., 2001;Steinbacher et al., 2004). While
480 previous studies reported decreases in benzene sensitivity by 16 – 56% from dry to
481 humid conditions (up to 100% RH), our results show a decrease of less than 1.1% per
482 10% RH increase (i.e., $< 11\%$ in the whole RH range) with a somewhat narrower RH



483 range (up to ~85% RH). In addition, two out of the three terpenoids (group A2) also
484 show slightly negative RH dependence, and the rest one (α -pinene) shows very small
485 positive RH dependence (Figure 5i). These hydrocarbons (aromatics and terpenoids) in
486 groups A1 and A2 have relatively low k_{ptr} values (mostly $<2.5 \times 10^{-9} \text{ cm}^3 \text{ molec}^{-1} \text{ s}^{-1}$,
487 Table S3), and their RH dependence shows a fairly good correlation with the PA value
488 (Figure 6a, purple circles and squares). This observation suggests that there might be a
489 thermodynamic reason behind the noticeable decrease of sensitivity for hydrocarbons
490 such as benzene as RH increases. Since hydrocarbons such as benzene and toluene do
491 not readily react with $\text{H}_3\text{O}^+(\text{H}_2\text{O})$ (Warneke et al., 2001), R1 is the main reaction to
492 form MH^+ . As water vapor concentration increases at high RH, the reverse reaction of
493 R1 might be important for compounds with low PA and low k_{ptr} values.



494
495 Figure 6: The RH dependence of MH^+ ion plotted against PA, color-coded by (a) k_{ptr}
496 and (b) f_{MH^+} .

497 Long-chain aldehydes (group B2) have the largest RH dependence of 1-4%
498 positive deviation per 10% RH increase for the MH^+ ions. The RH dependence of the
499 $[\text{MH} + \text{H}_2\text{O}]^+$ ions (Figure S15g) is even much higher (1.4–8.5% positive deviation per
500 10% RH increase). Interestingly, the trends of RH dependence for the MH^+ ions and
501 that for the $[\text{MH} + \text{H}_2\text{O}]^+$ ions for long-chain aldehydes are exactly opposite (Figure 5i
502 and Figure S15g); that is, pentanal > n-butanal > hexaldehyde. The reason behind this



503 observation is out of the scope of this study. The dominating $[\text{MH} - \text{H}_2\text{O}]^+$ ions for
504 long-chain aldehydes (Figure 2), however, show much less ($\pm 1\%$ per 10% RH increase)
505 RH dependence (Figure S16i). Other carbonyl compounds (groups B1, B3, B4, and B5)
506 also show positive deviations as RH increases (less than 1.5% increase in sensitivity
507 per 10% RH increase), albeit to various degrees (Figure 5i). Similar to long-chain
508 aldehydes, their $[\text{MH} + \text{H}_2\text{O}]^+$ ions also show a large positive deviation (Figure S16g),
509 and $[\text{MH} - \text{H}_2\text{O}]^+$ ions show little RH dependence (Figure S16e). These carbonyl
510 compounds have medium PA values (Figure 6a) except formaldehyde. If we exclude
511 formaldehyde (with an extremely low PA value, the up triangle to the far left in Figure
512 6b) and long-chain aldehydes (low percentages of MH^+ ions, $<25\%$, down triangles in
513 Figure 6b), the RH dependence of other carbonyl compounds shows a slightly
514 decreasing trend of RH dependence vs. PA values (Figure 6b, up triangles, left triangles,
515 right triangles, and double triangles). These observations might hint on the relationships
516 between the RH dependence of carbonyl compounds and reagent ion distribution as
517 well as reaction direction for R1-R4, which is different from those for pure
518 hydrocarbons (groups A1 and A2). Finally, the RH dependence of MH^+ for compounds
519 in groups C1 (nitriles) and C2 (methanol) is within $+1\%$ per 10% RH increase (Figure
520 5i).

521 Overall, in the whole RH range studied ($\sim 5\%$ to $\sim 85\%$), the RH dependence of
522 RH^+ ions for the 21 VOCs studied is less than 30%, with most compounds (except
523 group B2, long-chain aldehydes) less than 15%. For $[\text{MH} + \text{H}_2\text{O}]^+$ ions (mainly for
524 carbonyl compounds), strong RH dependence was observed (Figure S15), being 1.4 –
525 8.5% per 10% RH increase, or 8.9 – 63.2% from $\sim 5\%$ to $\sim 85\%$ RH. The dehydrated
526 ions ($[\text{MH} - \text{H}_2\text{O}]^+$), however, show the smallest RH dependence ($\pm 1\%$ per 10% RH
527 increase) among all the ions (Figure S16). Fragmented ions with decarbonization ($[\text{MH}$
528 $- \text{C}_x\text{H}_y]^+$) show mainly negative RH dependence, generally less than 3% per 10% RH
529 increase (Figure S17).

530 **4 Conclusions**

531 We investigated the response of protonated, adduct, and fragmented ions of 21
532 atmospherically relevant VOCs in a Vocus PTR-MS as instrument setting and RH
533 condition vary. For the two ways of increasing the E/N ratio, increasing the FIMR axial
534 voltage can substantially (by three to four orders of magnitude) increase sensitivity but



535 does not change the fractions of the MH^+ ions (mostly within 30%); reducing the FIMR
536 pressure, however, does not enhance sensitivity much but can lead to more substantial
537 fragmentation. Therefore, a high FIMR axial voltage of 600 – 700 volts and a medium
538 pressure of around 2.0 mbar are recommended. Increasing the RF amplitude of FIMR
539 can increase sensitivity by 1 to 1.5 orders of magnitude at 2.0 mbar and 1.5 to 2 orders
540 of magnitude at 3.5 mbar, and it does not change the MH^+ ion fractions (within 20%).
541 Therefore, a high RF amplitude of 500 V is recommended. Increasing the BSQ
542 amplitude does not increase the sensitivity much but changes the MH^+ ion fractions of
543 small ions substantially by changing the transmission efficiency. The choice of this
544 instrument setting mainly relies on what ions (i.e., those reagent ions with too high an
545 abundance) one wants to filter out. Our choice is at 300 V, which gives a 50%
546 transmission at about 55 Th.

547 The relationship between sensitivity and k_{ptr} is strongly affected by two factors: 1)
548 whether the MH^+ ion has a high transmission efficiency, and 2) whether the MH^+ ion
549 is the dominating ion. If so, a fairly good correlation ($R_{\text{Pr}} = 0.77$) was observed for the
550 VOCs studied. The transmission curve is also more reasonably resembling the sigmoid
551 function only if all the ions (protonated, adduct, and fragmented) are considered. The
552 low transmission efficiencies of formaldehyde and methanol result in extremely low
553 sensitivities of these two small OVOCs, although a low PA value is another reason for
554 the former.

555 As RH increases from ~5% to ~85%, the MH^+ ions for 19 out of the 21 VOCs
556 studied have sensitivity variation of less than 15%, but long-chain aldehydes have
557 positive RH dependence of up to 30%. The RH dependence of $[\text{MH} + \text{H}_2\text{O}]^+$ ions for
558 long-chain aldehydes is stronger, while that of the dominating $[\text{MH} - \text{H}_2\text{O}]^+$ ions is
559 limited. Therefore, the signal distributions among protonated, adduct, and fragmented
560 ions are also affected by RH variation. Together with their relatively high background
561 signals (especially for n-butanal, Figure S5b), quantification of long-chain aldehydes
562 in the ambient environment using Vocus requires special attention. It is also worth
563 noting that hydrocarbons generally show slight negative RH dependence, probably due
564 to their relatively low k_{ptr} values, although such RH dependence does not affect
565 quantification significantly; their RH dependence has a fairly good correlation with
566 their PA values, hinting a thermodynamic reason behind this trend.

567



568 **Competing interests**

569 At least one of the (co-)authors is a member of the editorial board of Atmospheric
570 Measurement Techniques

571 **Acknowledgments**

572 This work was supported by funding support from the Science and Technology
573 Development Fund, Macau SAR (File No. FDCT 0031/2023/AFJ) and a multiyear
574 research grant (No. MYRG2022-00027-FST) from the University of Macau.
575



576 References

- 577 Baasandorj, M., Millet, D. B., Hu, L., Mitroo, D., and Williams, B. J.: Measuring acetic and formic acid
578 by proton-transfer-reaction mass spectrometry: sensitivity, humidity dependence, and quantifying
579 interferences, *Atmos. Meas. Tech.*, 8, 1303-1321, <https://doi.org/10.5194/amt-8-1303-2015>, 2015.
- 580 Cappellin, L., Karl, T., Probst, M., Ismailova, O., Winkler, P. M., Soukoulis, C., Aprea, E., Märk, T. D.,
581 Gasperi, F., and Biasioli, F.: On Quantitative Determination of Volatile Organic Compound
582 Concentrations Using Proton Transfer Reaction Time-of-Flight Mass Spectrometry, *Environmental
583 Science & Technology*, 46, 2283-2290, <https://doi.org/10.1021/es203985t>, 2012.
- 584 Claflin, M. S., Pagonis, D., Finewax, Z., Handschy, A. V., Day, D. A., Brown, W. L., Jayne, J. T., Worsnop,
585 D. R., Jimenez, J. L., Ziemann, P. J., de Gouw, J., and Lerner, B. M.: An in situ gas chromatograph with
586 automatic detector switching between PTR- and EI-TOF-MS: isomer-resolved measurements of indoor
587 air, *Atmospheric Measurement Techniques* 14, 133-152, <https://doi.org/10.5194/amt-14-133-2021>, 2021.
- 588 Cui, L., Zhang, Z., Huang, Y., Lee, S. C., Blake, D. R., Ho, K. F., Wang, B., Gao, Y., Wang, X. M., and
589 Louie, P. K. K.: Measuring OVOCs and VOCs by PTR-MS in an urban roadside microenvironment of
590 Hong Kong: relative humidity and temperature dependence, and field intercomparisons, *Atmos. Meas.
591 Tech.*, 9, 5763-5779, <https://doi.org/10.5194/amt-9-5763-2016>, 2016.
- 592 de Gouw, J., and Warneke, C.: Measurements of volatile organic compounds in the earths atmosphere
593 using proton-transfer-reaction mass spectrometry, *Mass Spectrom Rev*, 26, 223-257,
594 <https://doi.org/10.1002/mas.20119>, 2007.
- 595 de Gouw, J. A., Goldan, P. D., Warneke, C., Kuster, W. C., Roberts, J. M., Marchewka, M., Bertman, S.
596 B., Pszenny, A. A. P., and Keene, W. C.: Validation of proton transfer reaction-mass spectrometry (PTR-
597 MS) measurements of gas-phase organic compounds in the atmosphere during the New England Air
598 Quality Study (NEAQS) in 2002, *Journal of Geophysical Research: Atmospheres*, 108,
599 <https://doi.org/10.1029/2003JD003863>, 2003.
- 600 Ellis, A. M., and Mayhew, C. A.: Chemical Ionization: Chemistry, Thermodynamics and Kinetics, in:
601 *Proton Transfer Reaction Mass Spectrometry*, 25-48, 2014.
- 602 Gueneron, M., Erickson, M. H., VanderSchelden, G. S., and Jobson, B. T.: PTR-MS fragmentation
603 patterns of gasoline hydrocarbons, *International Journal of Mass Spectrometry*, 379, 97-109,
604 <https://doi.org/10.1016/j.ijms.2015.01.001>, 2015.
- 605 Hansel, A., Jordan, A., Holzinger, R., Prazeller, P., Vogel, W., and Lindinger, W.: Proton transfer reaction
606 mass spectrometry: on-line trace gas analysis at the ppb level, *International Journal of Mass Spectrometry
607 and Ion Processes*, 149-150, 609-619, [https://doi.org/10.1016/0168-1176\(95\)04294-U](https://doi.org/10.1016/0168-1176(95)04294-U), 1995.
- 608 Hartungen, E. v., Wisthaler, A., Mikoviny, T., Jaksch, D., Boscaini, E., Dunphy, P. J., and Märk, T. D.:
609 Proton-transfer-reaction mass spectrometry (PTR-MS) of carboxylic acids: Determination of Henry's law
610 constants and axillary odour investigations, *International Journal of Mass Spectrometry*, 239, 243-248,
611 <https://doi.org/10.1016/j.ijms.2004.09.009>, 2004.
- 612 Inomata, S., Tanimoto, H., Kameyama, S., Tsunogai, U., Irie, H., Kanaya, Y., and Wang, Z.: Technical
613 Note: Determination of formaldehyde mixing ratios in air with PTR-MS: laboratory experiments and
614 field measurements, *Atmospheric Chemistry and Physics*, 8, 273-284, [https://doi.org/10.5194/acp-8-273-
615 2008](https://doi.org/10.5194/acp-8-273-2008), 2008.
- 616 Jensen, A., Liu, Z., Tan, W., Dix, B., Chen, T., Koss, A., Zhu, L., Li, L., and de Gouw, J.: Measurements
617 of Volatile Organic Compounds During the COVID-19 Lockdown in Changzhou, China, *Geophysical
618 Research Letters*, 48, e2021GL095560, <https://doi.org/10.1029/2021GL095560>, 2021.
- 619 Kari, E., Miettinen, P., Yli-Pirilä, P., Virtanen, A., and Faiola, C. L.: PTR-ToF-MS product ion
620 distributions and humidity-dependence of biogenic volatile organic compounds, *International Journal of
621 Mass Spectrometry*, 430, 87-97, <https://doi.org/10.1016/j.ijms.2018.05.003>, 2018.
- 622 Krechmer, J., Lopez-Hilfiker, F., Koss, A., Hutterli, M., Stoermer, C., Deming, B., Kimmel, J., Warneke,
623 C., Holzinger, R., Jayne, J., Worsnop, D., Fuhrer, K., Gonin, M., and de Gouw, J.: Evaluation of a New
624 Reagent-Ion Source and Focusing Ion-Molecule Reactor for Use in Proton-Transfer-Reaction Mass
625 Spectrometry, *Anal Chem*, 90, 12011-12018, <https://doi.org/10.1021/acs.analchem.8b02641>, 2018.
- 626 Li, H., Almeida, T. G., Luo, Y., Zhao, J., Palm, B. B., Daub, C. D., Huang, W., Mohr, C., Krechmer, J.
627 E., Kurtén, T., and Ehn, M.: Fragmentation inside proton-transfer-reaction-based mass spectrometers
628 limits the detection of ROOR and ROOH peroxides, *Atmos. Meas. Tech.*, 15, 1811-1827,
629 <https://doi.org/10.5194/amt-15-1811-2022>, 2022.
- 630 Lindinger, W., Hansel, A., and Jordan, A.: On-line monitoring of volatile organic compounds at pptv
631 levels by means of proton-transfer-reaction mass spectrometry (PTR-MS) medical applications, food
632 control and environmental research, *International Journal of Mass Spectrometry and Ion Processes*, 173,
633 191-241, [https://doi.org/10.1016/S0168-1176\(97\)00281-4](https://doi.org/10.1016/S0168-1176(97)00281-4), 1998.
- 634 Materić, D., Lanza, M., Sulzer, P., Herbig, J., Bruhn, D., Gauci, V., Mason, N., and Turner, C.: Selective



635 reagent ion-time of flight-mass spectrometry study of six common monoterpenes, *International Journal*
636 *of Mass Spectrometry*, 421, 40-50, <https://doi.org/10.1016/j.ijms.2017.06.003>, 2017.
637 Michoud, V., Sauvage, S., Léonardis, T., Fronval, I., Kukui, A., Locoge, N., and Dusanter, S.: Field
638 measurements of methylglyoxal using proton transfer reaction time-of-flight mass spectrometry and
639 comparison to the DNPH-HPLC-UV method, *Atmospheric Measurement Techniques*, 11, 5729-5740,
640 <https://doi.org/10.5194/amt-11-5729-2018>, 2018.
641 Pagonis, D., Sekimoto, K., and de Gouw, J.: A Library of Proton-Transfer Reactions of H₃O⁺ Ions Used
642 for Trace Gas Detection, *J Am Soc Mass Spectr*, 30, 1330-1335, [https://doi.org/10.1007/s13361-019-](https://doi.org/10.1007/s13361-019-02209-3)
643 [02209-3](https://doi.org/10.1007/s13361-019-02209-3), 2019.
644 Pleil, J. D., Hansel, A., and Beauchamp, J.: Advances in proton transfer reaction mass spectrometry
645 (PTR-MS): applications in exhaled breath analysis, food science, and atmospheric chemistry, *J Breath*
646 *Res*, 13, <https://doi.org/10.1088/1752-7163/ab21a7>, 2019.
647 Salazar Gómez, J. I., Sojka, M., Klucken, C., Schlögl, R., and Ruland, H.: Determination of trace
648 compounds and artifacts in nitrogen background measurements by proton transfer reaction time-of-flight
649 mass spectrometry under dry and humid conditions, *J Mass Spectrom*, 56, e4777,
650 <https://doi.org/10.1002/jms.4777>, 2021.
651 Schripp, T., Etienne, S., Fauck, C., Fuhrmann, F., Märk, L., and Salthammer, T.: Application of proton-
652 transfer-reaction-mass-spectrometry for Indoor Air Quality research, *Indoor Air*, 24, 178-189,
653 <https://doi.org/10.1111/ina.12061>, 2014.
654 Sekimoto, K., Li, S.-M., Yuan, B., Koss, A., Coggon, M., Warneke, C., and de Gouw, J.: Calculation of
655 the sensitivity of proton-transfer-reaction mass spectrometry (PTR-MS) for organic trace gases using
656 molecular properties, *International Journal of Mass Spectrometry*, 421, 71-94,
657 <https://doi.org/10.1016/j.ijms.2017.04.006>, 2017.
658 Sekimoto, K., and Koss, A. R.: Modern mass spectrometry in atmospheric sciences: Measurement of
659 volatile organic compounds in the troposphere using proton-transfer-reaction mass spectrometry, *J Mass*
660 *Spectrom*, 56, <https://doi.org/10.1002/jms.4619>, 2021.
661 Shao, P., An, J., Xin, J., Wu, F., Wang, J., Ji, D., and Wang, Y.: Source apportionment of VOCs and the
662 contribution to photochemical ozone formation during summer in the typical industrial area in the
663 Yangtze River Delta, China, *Atmospheric Research*, 176-177, 64-74,
664 <https://doi.org/10.1016/j.atmosres.2016.02.015>, 2016.
665 Shrivastava, M., Cappa, C. D., Fan, J., Goldstein, A. H., Guenther, A. B., Jimenez, J. L., Kuang, C.,
666 Laskin, A., Martin, S. T., Ng, N. L., Petaja, T., Pierce, J. R., Rasch, P. J., Roldin, P., Seinfeld, J. H.,
667 Shilling, J., Smith, J. N., Thornton, J. A., Volkamer, R., Wang, J., Worsnop, D. R., Zaveri, R. A., Zelenyuk,
668 A., and Zhang, Q.: Recent advances in understanding secondary organic aerosol: Implications for global
669 climate forcing, *Reviews of Geophysics*, 55, 509-559, <https://doi.org/10.1002/2016RG000540>, 2017.
670 Sinha, V., Custer, T. G., Kluepfel, T., and Williams, J.: The effect of relative humidity on the detection of
671 pyrrole by PTR-MS for OH reactivity measurements, *International Journal of Mass Spectrometry*, 282,
672 108-111, <https://doi.org/10.1016/j.ijms.2009.02.019>, 2009.
673 Smith, D., Diskin, A., Ji, Y. F., and Spänhel, P.: Concurrent use of H₃O⁺, NO⁺, and O-2(+) precursor ions
674 for the detection and quantification of diverse trace gases in the presence of air and breath by selected
675 ion-flow tube mass spectrometry, *INTERNATIONAL JOURNAL OF MASS SPECTROMETRY*, 209,
676 81-97, [https://doi.org/10.1016/S1387-3806\(01\)00478-X](https://doi.org/10.1016/S1387-3806(01)00478-X), 2001.
677 Španěl, P., and Smith, D.: SIFT studies of the reactions of H₃O⁺, NO⁺ and O₂⁺ with a series of volatile
678 carboxylic acids and esters, *International Journal of Mass Spectrometry and Ion Processes*, 172, 137-147,
679 [https://doi.org/10.1016/S0168-1176\(97\)00246-2](https://doi.org/10.1016/S0168-1176(97)00246-2), 1998.
680 Španěl, P., and Smith, D.: Selected ion flow tube: a technique for quantitative trace gas analysis of air
681 and breath, *Medical and Biological Engineering and Computing*, 34, 409-419,
682 <https://doi.org/10.1007/BF02523843>, 1996.
683 Španěl, P., Ji, Y., and Smith, D.: SIFT studies of the reactions of H₃O⁺, NO⁺ and O₂⁺ with a series of
684 aldehydes and ketones, *International Journal of Mass Spectrometry and Ion Processes*, 165-166, 25-37,
685 [https://doi.org/10.1016/S0168-1176\(97\)00166-3](https://doi.org/10.1016/S0168-1176(97)00166-3), 1997.
686 Španěl, P., and Smith, D.: Influence of water vapour on selected ion flow tube mass spectrometric
687 analyses of trace gases in humid air and breath, *Rapid Communications in Mass Spectrometry*, 14, 1898-
688 1906, [https://doi.org/10.1002/1097-0231\(20001030\)14:20<1898::AID-RCM110>3.0.CO;2-G](https://doi.org/10.1002/1097-0231(20001030)14:20<1898::AID-RCM110>3.0.CO;2-G), 2000.
689 Steinbacher, M., Dommen, J., Ammann, C., Spirig, C., Neftel, A., and Prevot, A. S. H.: Performance
690 characteristics of a proton-transfer-reaction mass spectrometer (PTR-MS) derived from laboratory and
691 field measurements, *International Journal of Mass Spectrometry*, 239, 117-128,
692 <https://doi.org/10.1016/j.ijms.2004.07.015>, 2004.
693 Vlasenko, A., Macdonald, A. M., Sjøstedt, S. J., and Abbatt, J. P. D.: Formaldehyde measurements by
694 Proton transfer reaction - Mass Spectrometry (PTR-MS): correction for humidity effects, *Atmospheric*



695 Measurement Techniques, 3, 1055-1062, <https://doi.org/10.5194/amt-3-1055-2010>, 2010.
696 Wang, Y., Yang, G., Lu, Y., Liu, Y., Chen, J., and Wang, L.: Detection of gaseous dimethylamine using
697 vocus proton-transfer-reaction time-of-flight mass spectrometry, Atmospheric Environment, 243, 117875,
698 <https://doi.org/10.1016/j.atmosenv.2020.117875>, 2020.
699 Warneke, C., van der Veen, C., Luxembourg, S., de Gouw, J. A., and Kok, A.: Measurements of benzene
700 and toluene in ambient air using proton-transfer-reaction mass spectrometry: calibration, humidity
701 dependence, and field intercomparison, International Journal of Mass Spectrometry, 207, 167-182,
702 [https://doi.org/10.1016/S1387-3806\(01\)00366-9](https://doi.org/10.1016/S1387-3806(01)00366-9), 2001.
703 Warneke, C., De Gouw, J. A., Kuster, W. C., Goldan, P. D., and Fall, R.: Validation of atmospheric VOC
704 measurements by proton-transfer-reaction mass spectrometry using a gas-chromatographic preseparation
705 method, Environ Sci Technol, 37, 2494-2501, <https://doi.org/10.1021/es026266j>, 2003.
706 Warneke, C., Veres, P., Holloway, J. S., Stutz, J., Tsai, C., Alvarez, S., Rappenglueck, B., Fehsenfeld, F.
707 C., Graus, M., Gilman, J. B., and de Gouw, J. A.: Airborne formaldehyde measurements using PTR-MS:
708 calibration, humidity dependence, inter-comparison and initial results, Atmos. Meas. Tech., 4, 2345-2358,
709 <https://doi.org/10.5194/amt-4-2345-2011>, 2011.
710 Yuan, B., Koss, A. R., Warneke, C., Coggon, M., Sekimoto, K., and de Gouw, J. A.: Proton-Transfer-
711 Reaction Mass Spectrometry: Applications in Atmospheric Sciences, Chemical Reviews, 117, 13187-
712 13229, <https://doi.org/10.1021/acs.chemrev.7b00325>, 2017.
713 Zhao, J., and Zhang, R.: Proton transfer reaction rate constants between hydronium ion (H₃O⁺) and
714 volatile organic compounds, Atmospheric Environment, 38, 2177-2185,
715 <https://doi.org/10.1016/j.atmosenv.2004.01.019>, 2004.